Zero valent nickel nanoparticles decorated polyaniline nanotubes for the efficient removal of Pb(II) from aqueous solution: Synthesis, characterization and mechanism investigation

Madhumita Bhaumik[a], Arjun Maity[b,c] and Hendrik G. Brink[a]

[a] Chemical Engineering Department, University of Pretoria, South Africa
[b] DST/CSIR, Centre for Nanostructure and Advanced Materials (CeNAM), Council for Scientific and Industrial Research (CSIR), Pretoria 0001, South Africa
[c] Department of Chemical Science, University of Johannesburg, Doornfontein, 2028 Johannesburg, South Africa

* Corresponding authors at: DST/CSIR, Centre for Nanostructure and Advanced Materials (CeNAM), Council for Scientific and Industrial Research (CSIR), Pretoria 0001, South Africa (A. Maity).

E-mail addresses: bhaumikmadhu@gmail.com (M. Bhaumik), amaity@csir.co.za (A. Maity), deon.brink@up.ac.za (H.G. Brink).

Highlights

•Novel composite nanotubes of polyaniline and Ni^0 NPs(PANI-NSA@Ni^0) were synthesized.
•Optimal removal of Pb(II) from aqueous solutions was achieved at pH 5.0.
•PANI-NSA@Ni^0 exhibited excellent removal capacity (414.6 mg/g at 25 °C) for Pb(II).
•Co-existing metal ions had substantial influence on Pb(II) removal performance.
•Adsorption of Pb(II) and its subsequent reduction were major removal mechanisms.

Abstract

Zero valent nickel nanoparticles (Ni^0 NPs) have exhibited potential applicability in various fields including, chemical cells, fuel cells and catalysis. Alike zero valent iron NPs, Ni^0 NPs and their composite nanostructures would have great prospect in remediating heavy metal pollutants from water bodies. To establish this fact composite nanotubes (CNs) of naphthalene sulfonic acid doped polyaniline (PANI-NSA) and Ni^0 NPs (PANI-NSA@Ni^0 CNs) were synthesized by immobilization of Ni^0 NPs onto the PANI-NSA surface and effectively used for the removal of Pb(II) ions from aqueous solution. Morphological and structural characterization established that aggregation of ferromagnetic Ni^0 NPs was greatly diminished by immobilization onto the matrix of PANI-NSA. Improved specific surface area and greater reactivity of the PANI-NSA@Ni^0 CNs enabled superior removal performance towards Pb(II) ions in comparison with its constituents. The highest removal efficiency (90.9%) was observed using 0.5 g/L CNs at pH 5.0. Pb(II) sorption kinetics was very rapid and equilibrium was reached within 30–90 min for 50–150 mg/L concentrations at pH 5.0. The Langmuir isotherm model provided the best description of the isotherm data, with a deduced maximum Pb(II) removal capacity of 414.6 mg/g at 25 °C. Thermodynamic analysis revealed exothermic and spontaneous adsorption onto the adsorbent surface. Co-existing heavy metal ions had slight impacts on Pb(II) removal performance of the PANI-NSA@Ni^0 with associated implications for the treatment of industrial wastewater. XRD and XPS

analyses allude that Pb(II) adsorption onto deprotonated surface sites followed by reduction to Pb^0 were the leading removal mechanism associated with the current CNs structure.

Graphical abstract

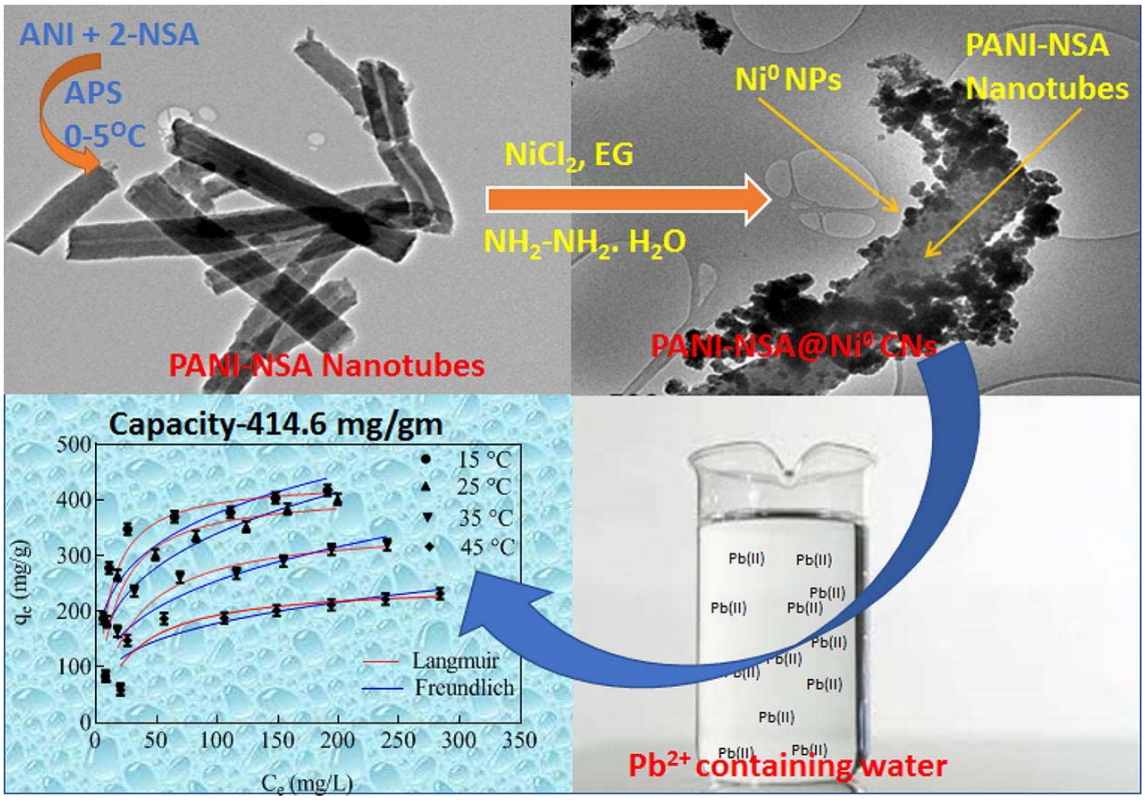

Keywords: Polyaniline nanotubes; Zero valent nickel nanoparticles; Nanocomposite; Adsorptive reduction; Kinetics; Thermodynamic

1. Introduction

Contamination of the aquatic environment by heavy metal pollutants e.g. chromium, mercury, arsenic, cadmium, copper, and lead etc. ions is one of the major environmental concerns encountered globally [1], [2], [3], [4]. Exposure to heavy metal contaminants, even at trace levels, leads to adverse health effects in human and other biological receptors. Amongst these heavy metals, lead in its ionic form i.e. Pb(II) is one of the most toxic in nature and is usually accrued in human bones, muscles, brain tissue, and kidneys resulting in diseases like anaemia, kidney damage, and neuronal disorders [5]. The discharge of wastewaters containing elevated concentrations of Pb(II) ions from industries such as electro plating, battery manufacturing, combustion of automobile fuel, paint and pigment manufacturing are the main contributors to the contamination of surface and ground water. Therefore, effective decontamination of toxic Pb(II) from industrial wastewater stream prior to release into natural water bodies is of prime importance. Several conventional treatment techniques such as chemical precipitation, reverse osmosis, ion exchange, bioremediation, and adsorption have been used for Pb(II) removal from water/wastewater [6], [7]. Inherent advantages including

simplicity of operation, high contaminant removal efficiency, and cost effectiveness have elevated adsorption as the most popular technique for the treatment of heavy metal laden wastewaters [8], [9]. The success of adsorption primarily depends on the selection of a suitable adsorbent with high adsorption affinity towards the target contaminant along with a rapid sorption rate. In this perspective nanomaterials possess high removal capacity of heavy metal ions from wastewater over conventional micro-scale adsorbents owing to their high specific surface area (surface/volume ratio) and highly reactive exposed surface sites [10]. Consequently, ever-increasing applications of nanomaterials in the wastewater treatment field have been observed over the previous two decades [11]. However, the application of nanomaterials, especially nanoparticles, in continuous flow systems such as fixed-bed and mixed vessels regularly experience severe limitations as a result of aggregation, difficulty in separation, and extreme pressure drop [12], [13], [14]. A simple methodology to prevent nanoparticle-aggregation is to support/immobilize these on porous support matrices and thereby forming well dispersed nanocomposites [15], [16]. Moreover, magnetic nanoparticles used to produce nanocomposites would have the advantage associated with easy separation form water after contaminant removal via simple application of an external magnetic field. Over the past several years various studies have explored the use of magnetic nano-composites for Pb(II) removal from aqueous solution [17], [18], [19]. Magnetic nanocomposites used for the treatment of aqueous Pb(II) are mostly based on nanoparticles of zero valent iron (metallic iron) and iron oxides [20], [21], [22], [23], [24]. Unlike metallic iron nanoparticles, investigations on other metallic nanoparticles e.g. metallic nickel (Ni^0) nanoparticles and its nanocomposite which could be used for the removal of heavy metals are not adequate.

Polyaniline (PANI), one of the most studied conducting polymers, has received tremendous attention for controllable synthesis of nanostructures because of its potential applications as supporting matrix for nanoparticles [25], [26]. Nanostructured PANI provides its wide applica-bility in nanoelectronics/nanodevices, anticorrosive coating, sensors, supercapacitors, and in catalysis [27], [28], [29], [30]. Furthermore, unique properties, including high specific surface area, good suspension ability and substantial affinity toward heavy metal ions, and an easy cost-effective bulk synthesis process for the production of PANI nanostructures have made it as an excellent adsorbent for application in separation and purification process [31], [32], [33]. Although a number of PANI based nanocomposites have been reported for Pb(II) sorption from water their adsorption capacities were limited [34], [35], [36], [37], [38], [39], [40]. Therefore, it is imperative to fabricate new PANI nanostructure-based adsorbent with superior affinity towards Pb(II) ions.

Herein, zero valent nickel nanoparticles (Ni^0 NPs) were supported/immobilized on naphthalene sulfonic acid (NSA) doped polyaniline (PANI-NSA) nanotubes surface to produce well dispersed magnetic nanocomposites for effective Pb(II) ions removal from aqueous solution. Synthesis of PANI-NSA@Ni^0 composite nanotubes (PANI-NSA@Ni^0 CNs) for the first time was performed through a facile two-step method. The field emission scanning electron microscopy (FE-SEM), high resolution transmission electron microscopy (HR-TEM), Brunauer–Emmett–Teller (BET) surface area measurement, X-ray powder diffraction (XRD), Fourier transform infrared spectroscopy (FTIR), X-ray photo electron spectroscopy (XPS) and vibrating sample magnetometer (VSM) techniques were employed for physico-chemical characterization of the prepared PANI-NSA@Ni^0 CNs. The performance of PANI-NSA@Ni^0 CNs towards Pb(II) removal from water was assessed through batch adsorption experiments. The impacts of solution initial pH, contact time, initial Pb(II) concentration and competing metal ions on removal of Pb(II) were investigated.

Mechanistic investigation for Pb(II) ions removal by PANI-NSA@Ni^0 CNs was also established in detail by analysing XRD and XPS data.

2. Materials and experimental methods

2.1. Materials

Aniline (ANI, 99%, Sigma Aldrich, USA)) monomer for polymerization to achieve PANI was purified by double distillation and stored at 0–5 °C prior to usage. 2-naphthalene sulfonic acid (2-NSA, 70%) as dopant, ammonium persulfate (APS, 98% purity) as oxidant, nickel(II) chloride hexahydrate, ethylene glycol (EG), hydrazine hydrate (50–60%), sodium hydroxide, nitric acid, lead(II) nitrate (>99.0%), zinc(II) nitrate hexahydrate (98%), cadmium(II) chloride (anhydrous > 99.0%) and copper(II) sulfate pentahydrate were also procured from Sigma Aldrich, USA and utilized as obtained.

2.2. Synthesis of PANI-NSA nanotubes

Nanotubes of 2-naphthalene sulfonic acid (2-NSA) doped PANI were synthesized according to the following method: 0.2 mL of ANI and 0.208 g of 2-NSA was mixed with 80 mL de-ionized water through stirring with magnetic stirrer at 0–5 °C. After 30 min of mixing, 10 mL of APS aqueous solution (0.456 g in 10 mL de-ionized water) was added to the 2-NSA-ANI mixture. Subsequently the mixing condition was sustained for further 1 min. Afterwards, the polymerization reaction mixture was preserved at 0–5 °C under static condition for 24 h. On accomplishment of polymer formation, 2-NSA doped PANI (PANI-NSA) was achieved through filtration, washing with deionized water and acetone followed by vacuum oven drying at 60 °C for 24 h.

2.3. Synthesis of PANI-NSA@Ni^0 CNs

The PANI-NSA@Ni^0 CNs were fabricated by immobilization/deposition of metallic Ni nanoparticles (Ni^0 NPs) onto the pre-synthesized PANI-NSA nanotubes surface/matrix. For deposition of the Ni^0 NPs onto the PANI-NSA nanotubes support, 0.2 g of PANI-NSA nanotubes powder was dispersed in 20 mL of a previously prepared ethylene glycol (EG)/Ni^{2+} ion solution (0.404 g $NiCl_2 \cdot 6H_2O$ dissolved in 20 mL EG) with mechanical agitation. Subsequently, to facilitate the reduction of Ni^{2+} ions to metallic Ni^0 NPs, 5 mL of hydrazine hydrate and 2 mL of a sodium hydroxide (1 M) solution were added to the above-mentioned dispersion. Reduction of Ni^{2+} ions by the reducing agent, hydrazine hydrate, leads to the formation of Ni^0 NPs on the PANI-NSA nanotubes matrix. The entire reduction process was performed in an oil bath maintained at 60 °C temperature. The synthesized PANI-NSA@Ni^0 CNs (~33.3 wt% Ni^0 loading) were separated, rinsed with water and ethanol, and finally dried under vacuum at 60 °C for 24 h. For comparison with PANI-NSA nanotubes and PANI-NSA@Ni^0 CNs, bare Ni^0 was also prepared by the reduction of Ni^{2+} using hydrazine hydrate reducing agent.

2.4. Characterization techniques

The morphology and size of the PANI-NSA nanotubes and PANI-NSA@Ni^0 CNs were evaluated by a scanning electron microscope equipped with a field emission electron gun (FE-SEM, Carl Zeiss, Germany) and a high-resolution (HR) transmission electron microscope (TEM), model-JEM-2100 from JEOL, Japan. The textural characterization of the

PANI-NSA@Ni^0 CNs, pristine PANI-NSA nanotubes and Ni^0 NPs were executed with a N_2 adsorption-desorption equipment (model-ASAP 2420) from Micromeritics, UK.

Structural (chemical) properties of the synthesized nanomaterials were assessed from the attenuated total reflection Fourier transform infrared (ATR-FTIR) spectra obtained by a PerkinElmer (USA) ATR-FTIR Spectrum 100 spectrometer. Crystalline behaviour of the PANI-NSA and PANI-NSA@Ni^0 CNs were explored by employing a PANalytical X'Pert PRO diffractometer. In order to examine the elemental constituents and oxidation state of the as grown Ni^0 NPs, PANI-NSA@Ni^0 were subjected to X-ray photoelectron spectroscopic (XPS) measurement on ESCALAB 250Xi XPS spectrometer from Thermo Scientific (USA) which uses an Al monochromatic X-ray source. The point-of-zero charge (PZC) of the PANI-NSA@Ni^0 CNs was determined by salt addition method [41]. The initial pH value at which the difference between final and initial pH (ΔpH) of the aqueous dispersion of PANI-NSA@Ni^0 CNs display zero was considered as the PZC. Magnetic measurement of the PANI-NSA@Ni^0 CNs was performed by Physical Property Measurements System (PPMS Evercool-II, Quantum Design, USA) with Vibrating Sample Magnetometer (VSM) measurement option.

2.5. Pb(II) removal experiments

Adsorption experimental solutions with required Pb(II) ions concentration were prepared by appropriate dilution of a 1000 mg/L stock solution. Equilibrium adsorption experimentations of Pb(II) were conducted by shaking the aqueous samples at 200 rpm in a thermostatic water bath shaker for 24 h. To assess the competitive removal performances, adsorption experiments were performed by contacting various doses of Ni^0 NPs, PANI-NSA and PANI-NSA@Ni^0 CNs adsorbents with 20 mL of 100 mg/L Pb(II) samples without pH adjustment (original solution pH 6.11) in 50 mL glass bottles. The influence of initial solution pH (ranging from 2.0 to 6.0) on Pb(II) removal efficiency was evaluated by mixing 0.01 g of PANI-NSA@Ni^0 CNs with 20 mL of 100 mg/L Pb(II) solutions for 24 h at 25 °C. The pH of the Pb(II) solutions was set to various values with the use of 0.1 M HNO_3 or 0.1 M NaOH. The Pb(II) ions adsorption efficiency (% removal) was calculated by employing Eq. (1):

$$\%\text{removal} = \left(\frac{C_0 - C_e}{C_0}\right) \times 100 \quad (1)$$

where C_0 and C_e are the initial and the equilibrium Pb(II) ions concentration (mg/L), respectively.

To study the temperature effect on Pb(II) adsorption capacity, isotherm data were produced by executing equilibrium experiments at respective temperatures 15, 25, 35 and 45 °C. For a specified temperature and at pH 5.0, the initial concentrations of Pb(II) ions were ranged between 50 mg/L to 400 mg/L. Other experimental parameters were similar to that of the pH effect experiment. The capacity for Pb(II) adsorption using PANI-NSA@Ni^0 CNs at equilibrium was determined through the application of Eq. (2):

$$q_e = \left(\frac{C_0 - C_e}{m}\right) V \quad (2)$$

In Eq. (2) q_e (mg/g) becomes the equilibrium adsorption capacity of an adsorbent; V (L) represents the sample volume; and m (g) is the adsorbent mass.

Kinetic experiments for Pb(II) removal were conducted by treating 0.1 g of PANI-NSA@Ni^0 CNs with 200 mL of Pb(II) ions solution (initial solution pH was adjusted to a value of 5.0) stirred with a speed of 200 rpm and set at 25 °C temperature. The initial Pb(II) ion concentrations were diverse from 50 to 150 mg/L. At pre-selected intervals of time 4 mL aliquots were withdrawn from the reaction vessel and filtered via 0.4 μm cellulose acetate syringe filters. The filtrate was analysed for residual Pb(II) concentrations using an Atomic Absorptions Spectrometer (AAnalyst-400 AA, PerkinElmer). The time-dependent Pb(II) adsorption capacity of PANI-NSA@Ni^0 CNs was determined by utilizing Eq. (3):

$$q_t = \left(\frac{C_0 - C_t}{m}\right) V \tag{3}$$

where, q_t (mg/g) denotes uptake (capacity) of Pb(II) per unit mass of the adsorbent at any selected time *t*, C_t (mg/L) specifies bulk-phase concentration of adsorbate ions at time t.

Experiment for the co-existing heavy metal ions effect on Pb(II) adsorption by PANI-NSA@Ni^0 CNs was performed in a multi-ions sorption mode. Studied co-existing heavy metal ions were: Pb(II), copper [Cu(II)], zinc [Zn(II)] and cadmium [Cd(II)], respectively. Accordingly, 20 mL aqueous solution containing all the studied heavy metal ions were contacted with 0.01 g of PANI-NSA@Ni^0 CNs for 24 h at 25 °C. In these multi-ions sorption systems initial concentrations for each of the co-existing metal ions were fixed at a value of 100 mg/L. After equilibration, the solutions were filtered and analysed for residual concentrations of Pb(II), Cu(II), Zn(II) and Cd(II), respectively. In addition, for comparison purpose adsorption performance (% removal) of the PANI-NSA@Ni^0 CNs towards all the studied metal ions were also tested in the absence of other competing heavy metal ions.

3. Results and discussion

3.1. Characterization

Morphological investigations of the prepared PANI-NSA nanotubes and PANI-NSA@Ni^0 CNs were performed by inspecting FE-SEM and HR-TEM images. Typical FE-SEM image of the pristine 2-NSA doped PANI polymer (PANI-NSA) is displayed in Fig. 1a. This image divulges the development of smooth surfaced nanotubes of PANI-NSA, 140–160 nm in diameter. However, due to the immobilization/deposition of spherical/nearly spherical Ni nanoparticles, the diameters of the PANI-NSA nanotubes increased to the 200–220 nm range (Fig. 1b) and the surface of the nanotubes appeared rougher.

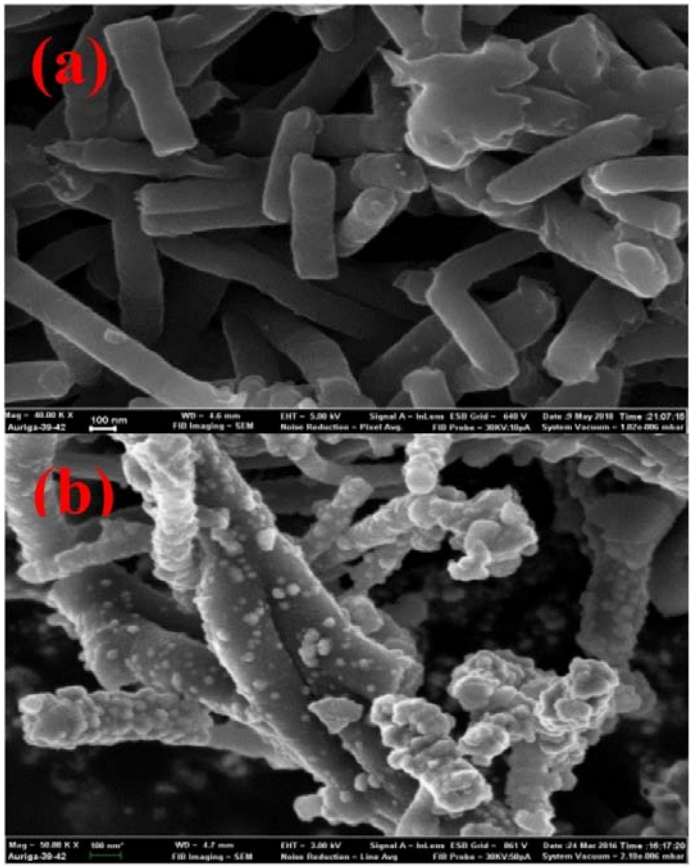

Fig. 1. FE-SEM images of (a) PANI-NSA nanotubes (b) PANI-NSA@Ni^0 CNs.

Fig. 2(a)–(c) represents the HR-TEM images of the PANI-NSA and PANI-NSA@Ni^0 CNs. It is evident from Fig. 2b that Ni^0 NPs are immobilized/deposited onto the smooth surface of PANI-NSA nanotubes (Fig. 2a) matrix.

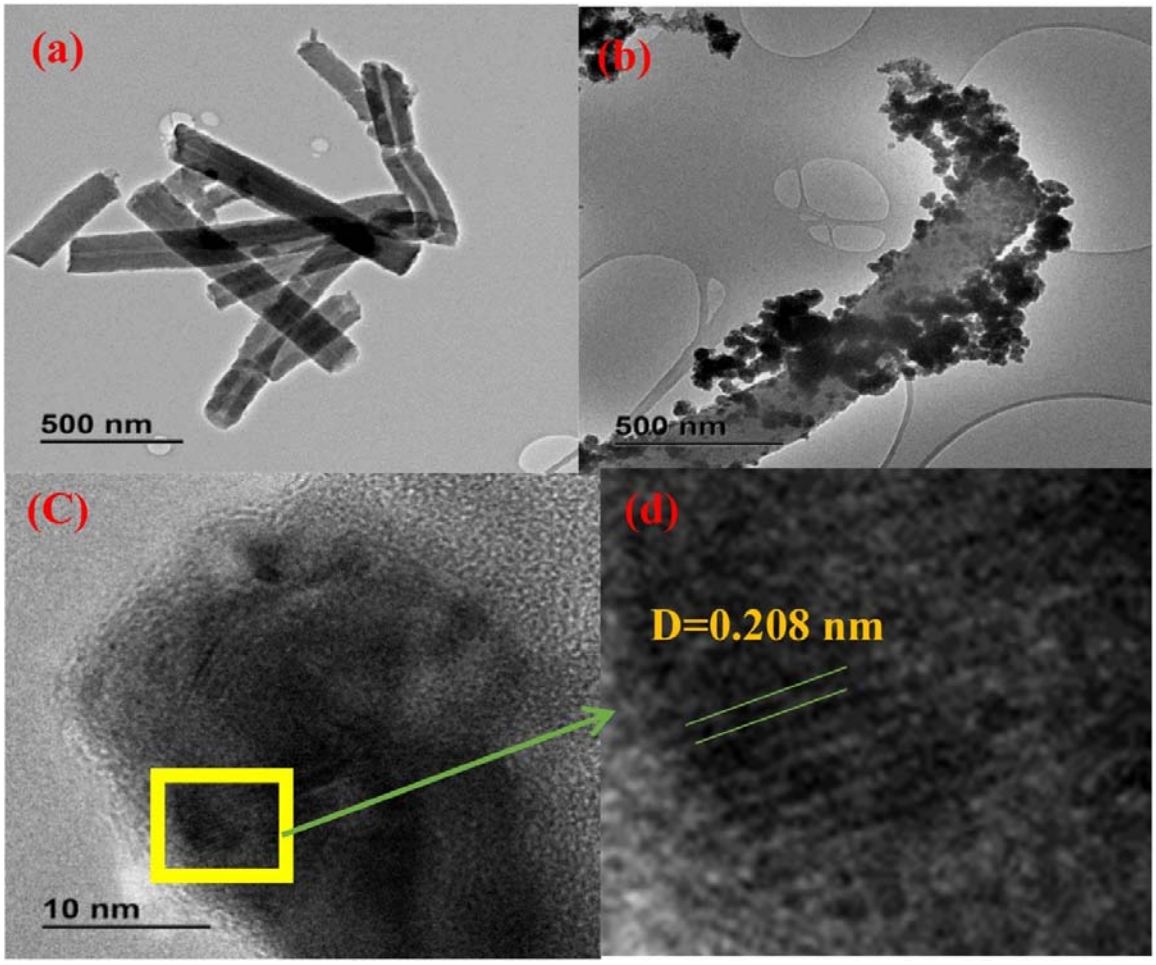

Fig. 2. HR-TEM images of (a) PANI-NSA nanotubes, (b) and (c) PANI-NSA@Ni^0 CNs at two different magnifications, (d) crystal lattice fringe of Ni^0 NPs in PANI-NSA@Ni^0 CNs.

The clear fringes of lattice with characteristic 0.208 nm inter planer spacing, as shown in the HR-TEM image (Fig. 2d) of PANI-NSA@Ni^0 CNs, resembled the face centred cubic (fcc) Ni^0 (1 1 1) crystal planes indicating a high crystallinity of the as grown Ni^0 NPs.

The Brunauer–Emmett–Teller (BET) specific surface area (S_{BET}) of the PANI-NSA@Ni^0 CNs, Ni^0 NPs and PANI-NSA nanotubes as obtained from N_2 adsorption-desorption isotherms (Fig. S1) are 49.84, 13.34 and 29.56 m^2/g, respectively. Substantial improvement in S_{BET} of the PANI-NSA@Ni^0 CNs compared to the PANI-NSA nanotubes and Ni^0 NPs counterparts indicates greater interfacial area will be available for the solid-liquid interaction to take place which apparently contributes towards superior contaminant removal performance. Additionally, from the pore size distribution result, calculated average pore width of the PANI-NSA@Ni^0 CNs, PANI-NSA nanotubes and Ni^0 NPs are as 6.5, 6.7 and 5.8 nm, respectively. The obtained averaged pore diameters are within the range of 2–50 nm representing mesoporous characteristic of the respective synthesized materials.

The X-ray diffraction (XRD) patterns of the PANI-NSA@Ni^0 CNs and bare PANI-NSA nanotubes are portrayed in Fig. 3a. The appearance of strong sharp diffraction peaks (Fig. 3a) at 2θ, of 44.7°, 52.1° and a small peak at 76.7° are the signature peaks of (1 1 1), (2 0 0) and

(2 2 0) crystal planes of metallic Ni (Ni^0) NPs (JCPDS cards No. 65-0380). This implies that Ni^0 NPs are effectively formed on the surface of PANI-NSA nanotubes. Moreover, the broad diffraction peaks of PANI-NSA nanotubes observed (Fig. 3a) at 2θ = 20.01° and 25.1° featuring amorphous nature of the polymer are also clearly detectable for PANI-NSA@Ni^0 CNs [42]. This result indicates that there might be a chemical interaction between the PANI-NSA nanotubes and deposited Ni^0 NPs. From the broadening of the diffraction peaks corresponding to (1 1 1) and (2 0 0) planes the average crystallite size of the supported Ni^0 NPs were calculated using Debye-Scherrer's formula and is found to be 11.68 nm.

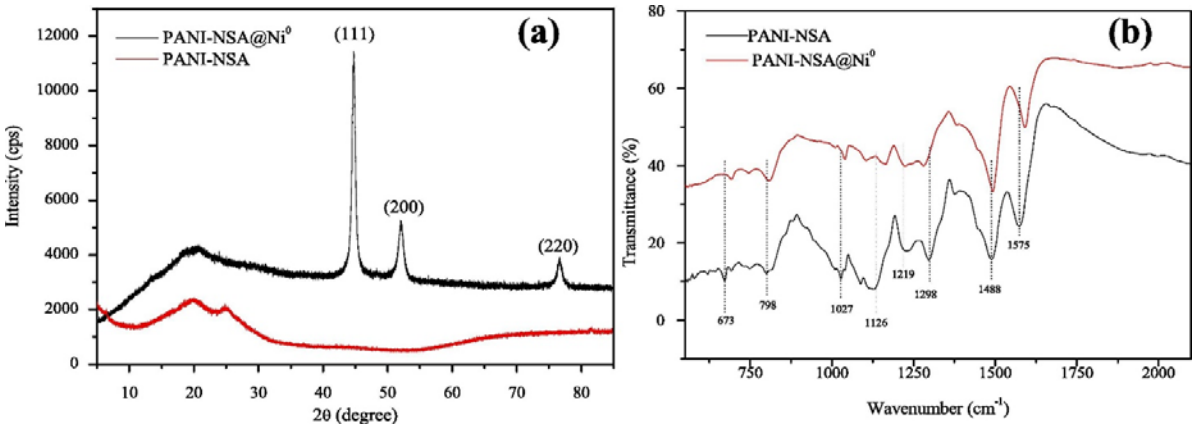

Fig. 3. (a) XRD patterns of PANI-NSA nanotubes and PANI-NSA@Ni^0 CNs and (b) ATR-FTIR spectra of PANI-NSA nanotubes and PANI-NSA/ Ni^0 CNs.

The chemical structure of the prepared PANI-NSA@Ni^0 CNs was characterized by analysing ATR-FTIR spectrum. The vibrational bands emerged at 1575 and 1488 cm^{-1} in the ATR-FTIR spectrum of Fig. 3b are the characteristic vibrational stretching associated with quinonoide (Q) and benzenoid (B) rings of PANI-NSA. The observed bands at 1298 and 1219 cm^{-1} are assigned to the stretching vibrations of the C–N bonds within Q-B-Q and B units while 1126 and 814 cm^{-1} frequency bands are the respective B-NH^+ = Q stretching, and C–H bending vibration of aromatic rings within the PANI backbone [43]. The doping of polymer with the sulfonic acid (−SO_3H) group of 2-NSA during polymerization was approved by the presence of bands at 1027 and 673 cm^{-1} in the FTIR-spectrum of PANI-NSA nanotubes [44]. Moreover, from Fig. 3b it can be perceived that all the characteristic FTIR peaks of PANI-NSA were red shifted to higher wave number after the formation of PANI-NSA@Ni^0 CNs.

Elemental compositions of the PANI-NSA@Ni^0 CNs and chemical oxidation state of the formed Ni^0 NPs were explored by XPS. Fig. 4a demonstrates the XPS survey spectrum of the PANI-NSA@Ni^0 CNs. Binding energy peaks of C 1s, N 1s, S 1s in the survey spectrum originated from the 2-NSA doped PANI moieties, whereas Ni 2p is assigned to the characteristic binding energy peak of deposited Ni species. These results recommend the existence of both Ni and 2-NSA doped PANI components in the synthesized CNs structure. Deconvoluted N 1s core level spectrum as depicted in Fig. 4b shows three binding energy peaks centred at 398.9 eV, 399.8 eV and 400.8 eV are attributed to doped imine (–NH^+=) units, amine (–NH–) of benzenoid, and cationic nitrogen atoms (–$NH^{\bullet+}$) i.e. polaron or bipolaron, respectively [45]. These findings confirm successful doping of PANI with 2-NSA. High resolution spectrum of Ni 2p (Fig. 4c) consists of two doublets of Ni $2p_{3/2}$ and Ni $2p_{1/2}$ arising from multi-electron excitations. The main peak of Ni $2p_{3/2}$ about 855.8 eV and the Ni

$2p_{1/2}$ peak around 873.5 eV along with their shake up satellite peaks (sat Ni $2p_{3/2}$ and sat Ni $2p_{1/2}$) suggest the presence of Ni^{2+} species on the PANI-NSA@Ni^0 CNs surface [46].

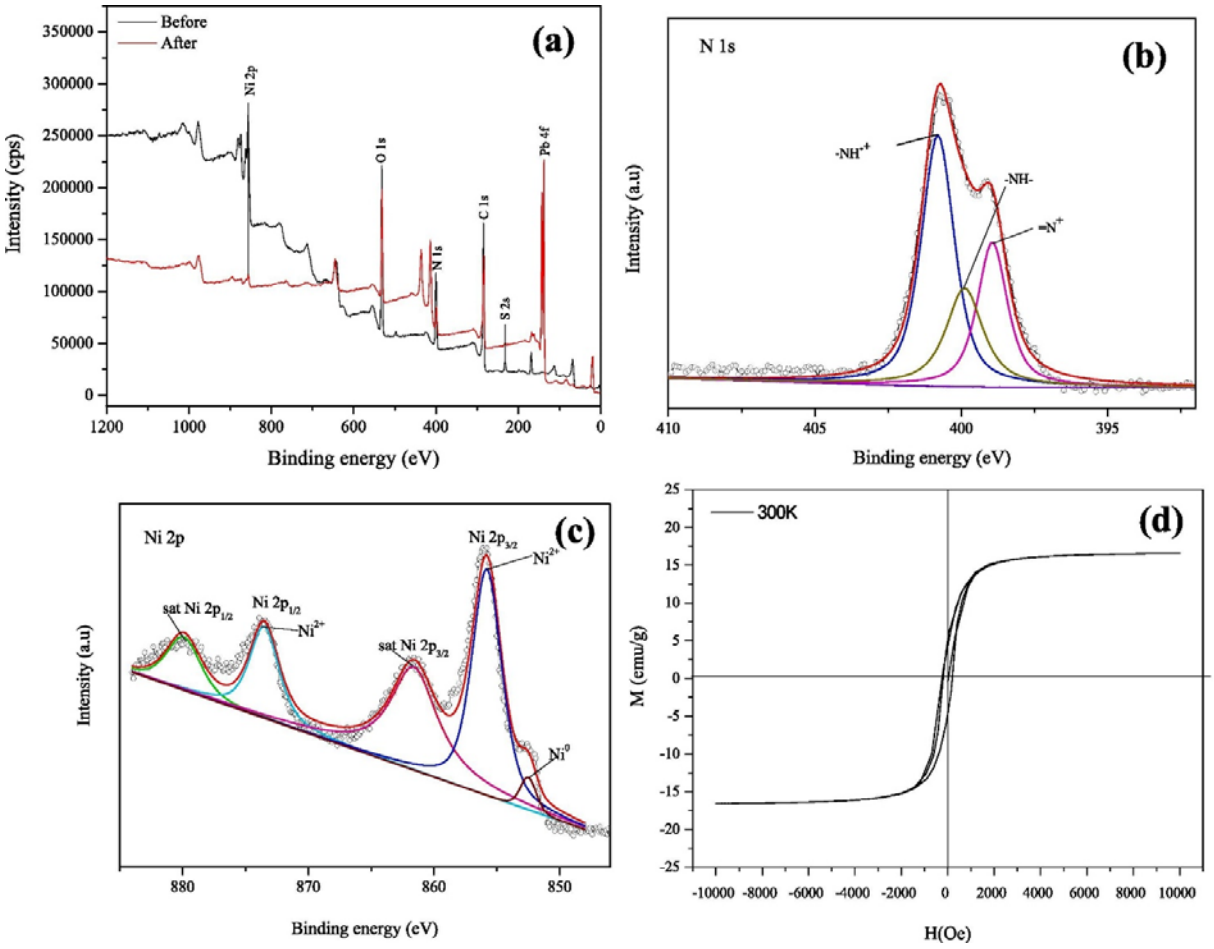

Fig. 4. (a) XPS survey spectra of the PANI-NSA@Ni^0 CNs before and after removal of Pb(II), (b) N1s core level spectrum of PANI-NSA@Ni^0 CNs, (c) Ni 2p spectrum of the PANI-NSA@Ni^0 CNs before Pb(II) removal and (d) M-H curve of the PANI-NSA@Ni^0 CNs at 300 K.

Furthermore, the Ni 2p peak with binding energy centred at 852.5 eV ($2p_{3/2}$) suggesting the presence of metallic Ni (Ni^0) NPs onto the surface of prepared nanotubes [46]. Detection of more Ni^{2+} species (either in the form of NiO or $Ni(OH)_2$) with more peak areas than metallic Ni (Ni^0) might be due to the high oxidation ability of the metallic Ni^0 NPs which formed a thin layer of Ni^{2+} species onto the nanotubes surface.

Magnetic hysteresis loop (M-H curve) of the PANI-NSA@Ni^0 CNs obtained at room temperature (300 K) is displayed in Fig. 4d. It is evident from the M-H curve that PANI-NSA@Ni^0 CNs possess weak ferromagnetic character with saturation magnetization (Ms) of 16.6 emu/g. The Ms value is considerably smaller than the Ms value of 55 emu/g Ni for bulk Ni at 300 K [47]. Presence of nonmagnetic (diamagnetic) PANI counterpart of the PANI-NSA@Ni^0 CNs may supress the M_S value to a certain extent.

3.2. Comparison of Pb(II) removal performance using various adsorbents

PANI-NSA@Ni^0 CNs along with PANI-NSA nanotubes and bare Ni^0 NPs were tested for the comparison of Pb(II) removal performances. Fig. 5a depicts the Pb(II) removal efficiencies (% removal) at various doses of PANI-NSA@Ni^0 CNs and its constituents. It can be evident from the Fig. 5a that highest percent (90.18%) of Pb(II) removal was achieved by PANI-NSA@Ni^0 CNs, whereas only 27.98% and 13.5% removal efficiencies were witnessed for Ni^0 NPs and PANI-NSA nanotubes, respectively, at a dose of 0.01 g/20 mL solution. This result indicates that Pb(II) removal from water using PANI-NSA@Ni^0 CNs was more efficient in comparison with bare Ni^0 NPs and PANI-NSA nanotubes counterparts. The superior performance of PANI-NSA@Ni^0 CNs toward Pb(II) removal is associated with its much larger specific surface area than PANI-NSA nanotubes and Ni^0 NPs. Additionally, as support matrix PANI-NSA nanotubes inhibited aggregation of magnetic Ni^0 NPs during composite formation and thereby providing increased reactivity towards Pb(II) adsorption [21]. The observed improved Pb(II) removal efficiencies with the increasing amount of each adsorbents is related with the increased number of active sites available for adsorption.

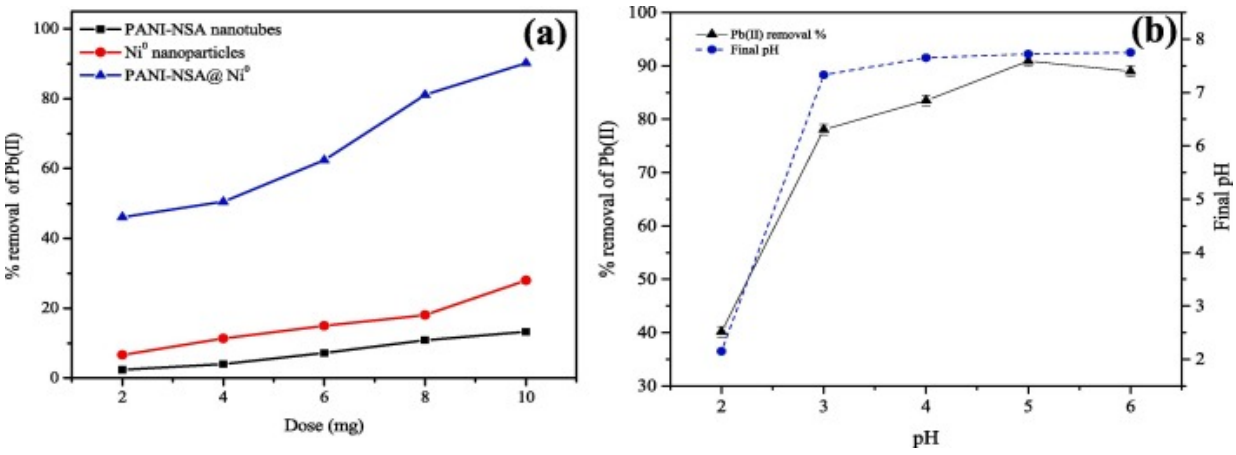

Fig. 5. (a) Comparison of Pb(II) removal performances using PANI-NSA nanotubes, Ni^0 NPs and PANI-NSA@Ni^0 CNs at different doses (Initial concentration: 100 mg/L, pH: 5.11) and (b) Effect of pH on adsorption of Pb(II) by PANI-NSA@Ni^0 CNs (Initial conc.: 100 mg/L, dose: 0.5 g/L).

3.3. Effect of initial pH

Initial pH of the metal ions solution is one of the prime factors greatly influencing the adsorption process. This is due to the facts that it determines the charged species to be formed at the surface of the adsorbent and controls the interactions amongst adsorbate ions and surface species of the sorbent. The influence of initial solution pH on Pb(II) removal performance by PANI-NSA@Ni^0 CNs is shown in Fig. 5b. The final pH value of the solutions after Pb(II) removal are also presented in Fig. 5b. The increase in initial solution pH from 2.0 to 2.15, 3.0 to 7.33, 4.0 to 7.65, 5.0 to 7.72 and 6.0 to 7.75 is principally from oxidation of Ni^0 to Ni^{2+} species by water and by dissolved oxygen [48]. The Pb(II) removal efficiency (% removal) of PANI-NSA@Ni^0 CNs was considerably lower between the pH range 2–3, whereas significant increase in removal efficiency was attained within the range of pH 4–6.

Variation of the initial pH between 5 and 6 had a minor effect on Pb(II) removal efficiency (Fig. 5b); as the efficiency of removal changed from 90.91% at pH 5 to 88.98% when the pH

value was 6. This variation in Pb(II) removal performance at different initial pH of the solution can be explained by considering PZC value of the adsorbent, which is at pH 4.44 as depicted in Fig. S2. The surface of the PANI-NSA@Ni^0 CNs adsorbent becomes positively charged (protonated) below the pH of PZC (pH_{PZC}) and exceeding it the surface remains deprotonated or negatively charged. Consequently, in the lower pH range ($pH < pH_{PZC} = 4.44$) electrostatic repulsion of positively charged surface as well as competitive interaction between protons (H^+) and Pb(II) ions leads to reduced Pb(II) removal efficiency of the PANI-NSA@Ni^0 CNs adsorbent [22]. On the contrary, at higher pH ($pH > 4.44$) negatively charged (deprotonated) surface of the adsorbent favours higher Pb(II) removal efficiency. Meanwhile, possible formation of Ni^{2+} and Pb(II) oxyhydroxide precipitation onto the surface of the PANI-NSA@Ni^0 CNs might have resulted slightly lesser removal efficiency at pH 6.0. This result corroborates that the optimal removal of Pb(II) by PANI-NSA@Ni^0 CNs was achieved at pH 5.0.

3.4. Sorption kinetics

The kinetic behaviour of the PANI-NSA@Ni^0 CNs towards Pb(II) removal is depicted in Fig. 6 for three different initial concentrations. Rapid sorption of Pb(II) by PANI-NSA@Ni^0 CNs is perceived with increased adsorption capacity associated with increases in initial concentrations. Additionally, equilibrium time varied from 30 to 90 min for the change in initial Pb(II) ion concentrations from 50 mg/L to 150 mg/L. Faster removal rate for Pb(II) ions is experienced from the highly reactive exposed surface sites of the PANI-NSA@Ni^0 CNs with larger specific surface area.

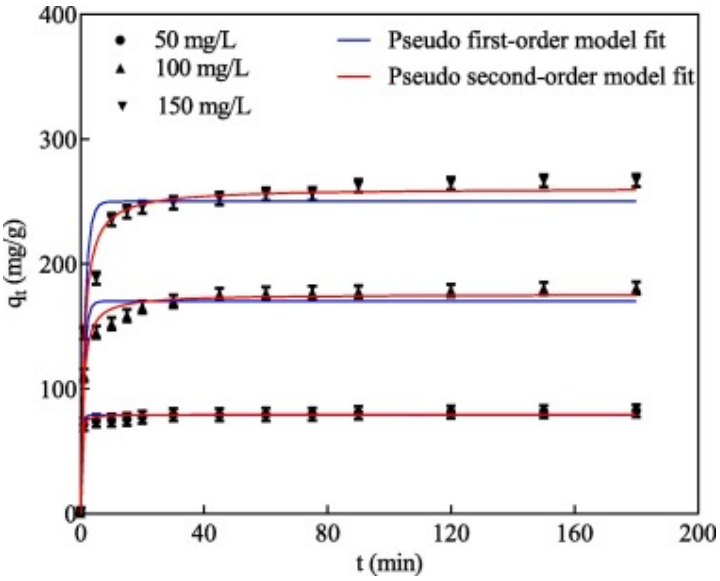

Fig. 6. The effect of contact time on adsorption of Pb(II) by PANI-NSA@Ni^0 CNs and the fitting of kinetic data with non-linear pseudo-first-order and pseudo-second-order kinetic models (dose: 0.5 g/L, pH: 5.0).

Evaluation of the kinetic mechanism for Pb(II) sorption was performed by analysing the experimentally obtained kinetic data with two widely used kinetic models namely; pseudo-first-order and pseudo-second-order kinetic models. The pseudo-first-order and pseudo-second-order kinetic models with their non-linear forms can be represented by the following Eqs:

$$\frac{dq_t}{dt} = k_1(q_e - q_t) \quad (4)$$

$$\frac{dq_t}{dt} = k_2(q_e - q_t)^2 \quad (5)$$

where k_1 and k_2 are the representative of rate constants for pseudo-first-order and pseudo-second-order kinetic models, respectively. The fittings of kinetic data with Eqs. (4), (5) are also presented in Fig. 6. The rate constants along with the correlation coefficients (R^2) as determined from the non-linear plots are given in Table 1. The pseudo-second-order model generated higher values of the R^2 (≈ 0.982–0.990) when compared with R^2 values for pseudo-first-order model (R^2 ≈ 0.933–0.986) suggesting its better validation in explaining the experimental kinetic data. The q_e values as obtained from both pseudo-second-order model fitting and from experiments are in good agreement which further suggests participation of this kinetic mechanism in the current Pb(II) removal process.

Table 1. Kinetics parameters of Pb(II) removal using PANI-NSA@Ni^0 CNs.

Kinetic model	**Initial Concentration**		
	50 mg/L	**100 mg/L**	**150 mg/L**
Pseudo-first-order			
Best-fit values			
q_e	78.87	170.1	250.2
K_1	2.367	1.022	0.7344
Std. Error			
q_e	0.7482	3.280	5.710
K_1	0.3624	0.1879	0.1607
95% Confidence Intervals			
q_e	77.24 to 80.50	163.0 to 177.3	237.7 to 262.6
K_1	1.578 to 3.157	0.612 to 1.431	0.3841 to 1.085
Goodness of Fit			
Degrees of Freedom	12	12	12
R^2	0.9862	0.9492	0.9339
Absolute Sum of Squares	80.61	1533	4552
Sy.x	2.592	11.30	19.48
Number of Points Analyzed	14	14	14
Pseudo-second-order			
Best-fit values			
q_e	79.45	175.7	260.8
K_2	0.09406	0.00798	0.003712
Std. Error			
q_e	0.6710	2.158	3.499
K_2	0.02632	0.00124	0.000561
95% Confidence Intervals			
q_e	77.99 to 80.91	171.0 to 180.4	253.1 to 268.4

Kinetic model	Initial Concentration		
	50 mg/L	100 mg/L	150 mg/L
K_2	0.03670 to 0.1514	0.00528 to 0.01069	0.00248 to 0.00496
Goodness of Fit			
Degrees of Freedom	12	12	12
R^2	0.9903	0.9832	0.9821
Absolute Sum of Squares	56.54	508.6	1234
Sy.x	2.171	6.510	10.14
Number of Points Analyzed	14	14	14

Units: q_e: mg/g, K_1: 1/min, K_2: g/mg.min.

3.5. Adsorption isotherm

Equilibrium isotherm data is a prerequisite for the determination of the maximum adsorption capacity of an adsorbent. This is also vital for the design and successful operation of an adsorption system. The equilibrium isotherm data acquired at four different temperatures (15, 25, 35 and 45 °C) for Pb(II) adsorption onto PANI-NSA@Ni^0 CNs are exhibited in Fig. 7.

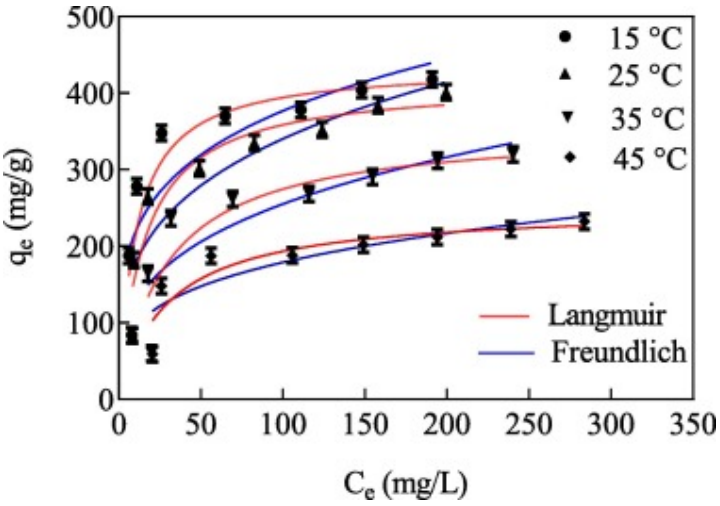

Fig. 7. Equilibrium isotherms of Pb(II) adsorption onto PANI-NSA@Ni^0 CNs and non-linear fitting of isotherm data with Langmuir and Freundlich models (Initial conc.: 50–400 mg/L, dose: 0.5 g/L and pH: 5.0).

It can be noted from the Fig. 7 that the capacity of the adsorbent towards Pb(II) adsorption increases with decrease in temperature which suggests exothermicity of the present adsorption process. Meanwhile, to examine the experimental isotherm data commonly used Langmuir and Freundlich isotherm models were utilized. The Langmuir and Freundlich isotherm models with their non-linear and linear forms are articulated by Eqs. (6)–(9), respectively:

$$q_e = \frac{q_m b C_e}{1+bC_e} \quad (6)$$

$$\frac{C_e}{q_e} = \frac{1}{q_m b} + \frac{C_e}{q_m} \quad (7)$$

$$q_e = K_F C_e^{1/n} \quad (8)$$

$$\ln q_e = \ln k_F + \frac{1}{n} \ln C_e \quad (9)$$

where q_m (mg/g) denotes maximum adsorption capacity of the adsorbent; b (L/mg) signifies free energy of sorption; k_F ((mg/g)(L/mg)$^{1/n}$) becomes Freundlich isotherm constant related with adsorption capacity and n is the intensity of adsorption, respectively. The non-linear and linear Langmuir and Freundlich isotherm models fitting to the isotherm data are demonstrated in Figs. 7 and S3(a and b), respectively. The isotherm model parameters as acquired from linear and non-linear regression analyses of the experimental data at four different temperatures are presented in Table 2. Superior competency of Langmuir model in describing the isotherm data is confirmed by the relative larger values of correlation coefficients (R^2) for both linear and non-linear Langmuir model than that of Freundlich model. This further suggests that Pb(II) adsorption is governed by the monolayer formation mechanism onto the homogeneous surface sites of the PANI-NSA@Ni^0 CNs. The q_m value for Pb(II) adsorption onto the PANI-NSA@Ni^0 CNs decreases from 434.7 (or 435.4 for non-linear fit) to 243.9 (or 250.3 for non-linear fit) mg/g with a variation in temperature from 15 to 45 °C. These results imply that at lower temperature the chemical interaction amongst active sorption sites of the adsorbent and Pb(II) ions is improved. Likewise, the b value decreases from 0.122 (0.095 for non-linear fit) to 0.043 (0.033 for non-linear fit) as temperature is increased from 15 to 45 °C, indicating the greater affinity of the PANI-NSA@Ni^0 CNs towards Pb(II) at reduced temperature. The maximum adsorption capacity of the PANI-NSA@Ni^0 CNs for Pb(II) removal is compared with various PANI based composite materials recently reported in the literature [34], [35], [36], [37], [38], [39], [40] and are listed in Table 3. The maximum Pb(II) adsorption capacity (q_m) PANI-NSA@Ni^0 CNs is significantly higher than the reported PANI based composite materials. Superior adsorption capacity, facile cost-effective synthesis of the PANI-NSA@Ni^0 CNs further recommend its prospective application in industrial wastewater treatment plants.

Table 2. Langmuir and Freundlich isotherm model parameters for Pb(II) adsorption by the PANI-NSA@Ni^0 composite nanotubes.

Isotherm Model	**Temperature**			
	15 °C	**25 °C**	**35 °C**	**45 °C**
Langmuir				
Linear				
q_m	434.7	416.67	344.82	243.90
b	0.1229	0.0641	0.0482	0.0432
R^2	0.9978	0.9940	0.9946	0.9940
Non-linear				
Best-fit values				
q_m	435.4	414.6	355.7	250.3
b	0.0954	0.0638	0.0338	0.0339
Std. Error				
q_m	35.39	26.45	39.45	20.42
b	0.0399	0.0172	0.0139	0.0117

Isotherm Model	Temperature			
	15 °C	**25 °C**	**35 °C**	**45 °C**
95% Confidence Intervals				
q_m	355.7–529.6	355.5–488.2	275.0–484.2	207.4–310.5
b	0.042 to 0.235	0.328 to 0.125	0.012 to 0.102	0.015 to 0.084
Goodness of Fit				
Degrees of Freedom	6	6	6	6
R^2	0.8316	0.9081	0.7929	0.8316
Absolute Sum of Squares	16,365	7564	11,043	3546
Sy.x	52.23	35.51	42.90	24.31
Number of Points Analyzed	8	8	8	8
Freundlich				
Linear				
k_F	157.52	121.87	90.74	88.27
n	5.133	4.401	4.545	5.931
R^2	0.8472	0.9389	0.8931	0.9422
Non-Linear				
k_F	125.7	91.53	61.13	49.75
n	4.195	4.195 3.508	3.224	3.599
Std. Error				
k_F	36.17	23.31	25.40	18.07
n	1.145	0.681	0.894	0.938
95% Confidence Intervals				
k_F	56.32 to 229.2	46.01 to 157.8	19.31 to 147.2	18.76 to 108.3
n	2.433 to 10.53	2.324 to 6.142	1.849 to 8.256	2.140 to 8.453
Goodness of Fit				
Degrees of Freedom	6	6	6	6
R^2	0.7422	0.8599	0.7397	0.8652
Absolute Sum of Squares	25,051	11,537	13,878	5106
Sy.x	64.62	43.85	48.09	29.17
Number of Points Analyzed	8	8	8	8

Units: q_m: mg/g, b: L/mg, K_F: ((mg/g)(mg/L)$^{-1/n}$.

Table 3. Comparison of Pb(II) maximum adsorption capacity (q_m) of the PANI-NSA@Ni^0 composite nanotubes with other PANI based adsorbents.

Adsorbents	q_m (mg/g)	Optimum pH	Temperature	References
Polyaniline/multi walled carbon nanotubes	22.2	5.0	20 °C	[34]
Polyaniline-Chitosan composite	16.07	3.0	30 °C	[35]
Polyaniline-Chitin	7.03	6.0	30 °C	[36]
Polyaniline-Clay nanocomposite	70.42	4.0	_	[37]
Polyaniline-polystyrene composite nanofibers	28.17	5.0	_	[38]
Polyaniline/$CoFeC_6N_6$ nanocomposite	18.34	neutral	25 °C	[39]
Polyaniline/TiO_2	95.24	5.0	25 °C	[40]
PANI-NSA@Ni^0 composite nanotubes	414.6	5.0	25 °C	[Present study]

3.6. Investigation of thermodynamic parameters

Three commonly studied thermodynamic parameters including standard Gibbs free energy change (ΔG^0), entropy change (ΔS^0) and change in enthalpy (ΔH^0) for Pb(II) adsorption onto PANI-NSA@Ni^0 CNs were acquired by employing Eqs. (6), (7):

$$\Delta G^{\circ} = -RT\ln K_c \tag{10}$$

$$\ln K_c = \frac{\Delta S^0}{R} - \frac{\Delta H^0}{RT} \tag{11}$$

where R is the universal gas constant in (J/mol/K), T (K) stands for temperature in absolute scale and K_c is referred to as the thermodynamic equilibrium constant. The ln Kc vs 1/T graph to determine all the three above mentioned thermodynamic parameters is presented in Fig. S4. The obtained values of the all three thermodynamic parameters are given in Table 4.

Table 4. Thermodynamic parameters for the removal of Pb(II) by PANI-NSA@Ni^0 composite nanotubes.

Temp (°C)	$\Delta G°$ (kJ/mol)	$\Delta H°$ (kJ/mol)	$\Delta S°$ (kJ/mol/K)
15	–2.935	–28.968	–0.0895
25	–2.588		
35	–1.614		
45	–0.231		

The negative value of ΔH^0 alludes an exothermic nature of the present adsorption process. This further indicates that the Pb(II) adsorption by PANI-NSA@Ni^0 CNs was favourable at lower temperature than that at higher temperature. Meanwhile, spontaneous sorption of Pb(II) ions onto the surface of the adsorbent is corroborated with the negative values of ΔG^0.

Finally, negative value of ΔS^0 is indicative of decrease in randomness at the solid-liquid interface for this adsorption scheme.

3.7. Effect of co-existing metal ions

Several industries including automotive, electroplating, battery manufacturing, aeronautical, and steel discharge wastewater containing considerable amount of Pb(II) along with other heavy metal ions such Cu(II), Zn(II) and Cd(II) etc. Therefore, the effects of these co-contaminating metal ions on Pb(II) adsorption by PANI-NSA@Ni^0 CNs were tested in a multi-ions sorption mode. Various metal ions (Pb(II), Cu(II), Zn(II) and Cd(II)) removal efficiencies (% removal) of PANI-NSA@Ni^0 CNs from single ion and multi-ions sorption systems are presented in Fig. 8. It is obvious from the Fig. 8 that in the absence of other co-contaminating metal ions ~90.9% of Pb(II), 18.7% of Cu(II), 43.4% of Zn(II) and 12.1% of Cd(II) were removed from aqueous solution with 100 mg/L (20 mL) initial concentration using 0.01 g of PANI-NSA@Ni^0 CNs. In contrast, reduced removal efficiencies are identified for all the studied metal ions in multi-ions sorption system. Precisely, decrease in Pb(II) removal efficiency from 90.9 to 85.9%, 18.7 to 14.2% for Cu(II), 43.4 to 9.2% for Zn(II) and 12.1 to 3.7% for Cd(II) can be perceived from Fig. 8. This result suggests the competitive influence of other metal ions on Pb(II) removal performance which follows the order of Pb(II) > Cu(II) > Zn(II) > Cd(II). Minor reduction in Pb(II) removal efficiency in presence of co-existing metal ions affirms potential applicability of PANI-NSA@Ni^0 CNs for the decontamination of industrial wastewater.

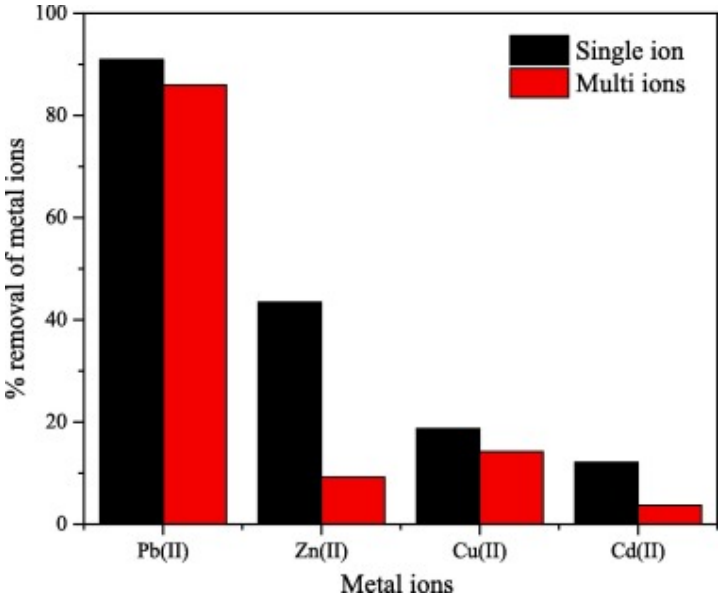

Fig. 8. Effect of co-existing metal ions on the adsorption of Pb(II) onto PANI-NSA@Ni^0 CNs (Initial Pb(II) + Cu(II) + Zn(II) + Cd(II) conc.: 100 mg/L, dose: 0.5 g/L and pH: 5.0).

3.8. Investigation of Pb(II) removal mechanism

In order to investigate the removal mechanism of Pb(II) from aqueous solution using PANI-NSA@Ni^0 CNs, XRD and XPS analyses results were employed. The XRD pattern of PANI-NSA@Ni^0 CNs after reaction with Pb(II) as shown in Fig. 9a exposes a variation in characteristic diffraction peaks when compared with the XRD peaks (Fig. 3a) prior to

reaction. The peaks appeared at 2θ of 24.31°and 32.47° resembled with the $Pb(OH)_2$ and the peak at 33.6° is in conformity with crystalline peak of $PbO{\cdot}xH_2O$.

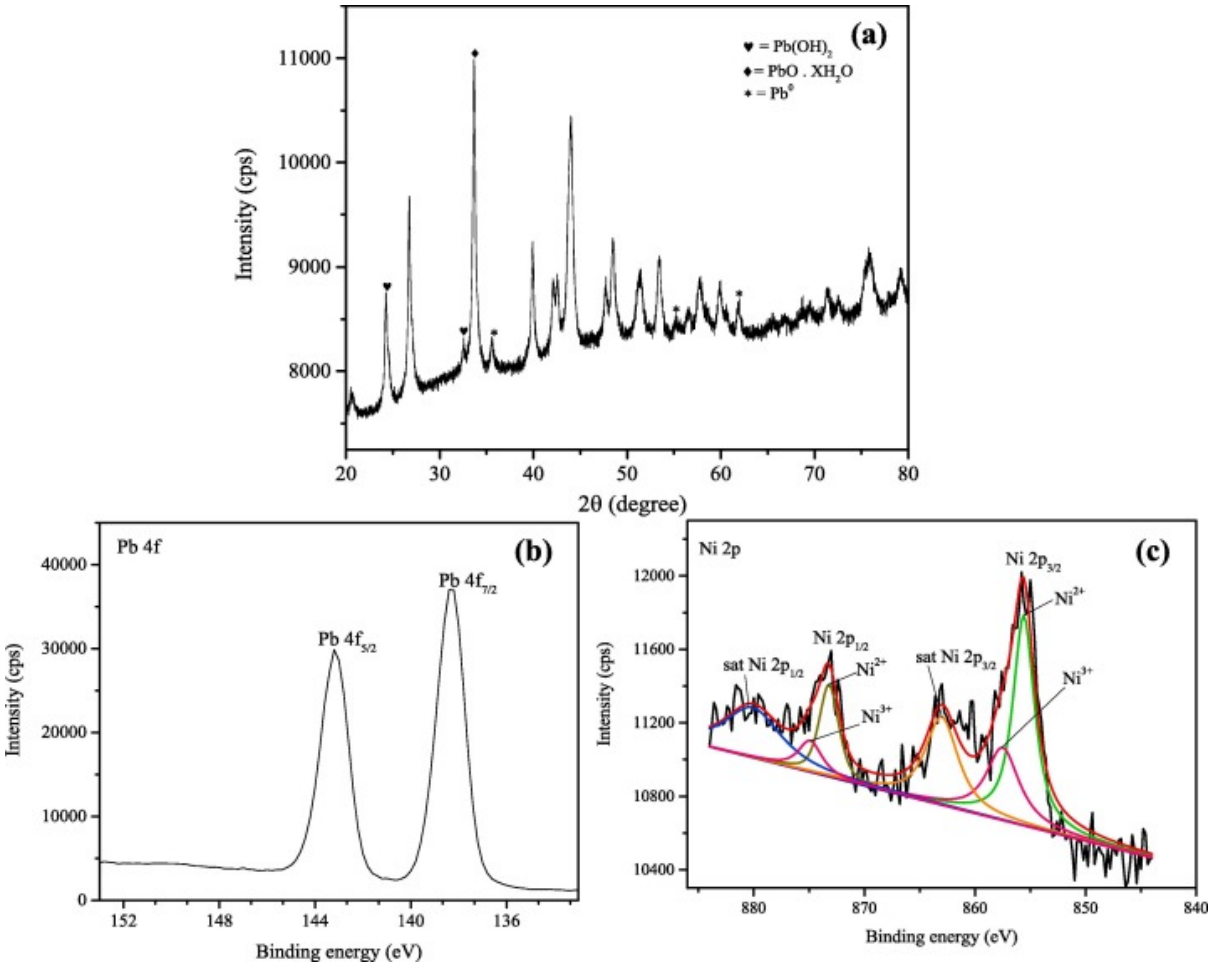

Fig. 9. (a) XRD pattern of the PANI-NSA@Ni^0 CNs after removal of Pb(II), (b) high resolution XPS spectra of Pb 4f, and (c) Ni 2p after removal of Pb(II) by PANI-NSA@Ni^0 CNs.

Meanwhile, characteristic diffraction peaks at 2θ value of 35.5°, 55.2° and 62.06° are associated with the metallic Pb or Pb^0 [20]. Therefore, the XRD results suggest that in aqueous medium at higher pH (~5.0) oxidation of Ni^0 into Ni^{2+} leads to the adsorption of Pb(II) and its conversion into $Pb(OH)_2$ and $PbO{\cdot}xH_2O$. Additionally, electrochemical reduction of Pb(II) species produces Pb^0 as a result of the fact that the standard reduction potential of Ni^{2+}/Ni^0 is −0.257 V, more negative than that of Pb^{2+}/Pb^0 which is −0.1263 V [21]. These electrochemically reduced Pb^0 were immobilized onto the surface of the PANI-NSA@Ni^0 composite nanotubes as observed in the XRD pattern. The XPS survey spectrum of the PANI-NSA@Ni^0 CNs after treatment with aqueous Pb(II) is shown in Fig. 4a. Appearance of Pb 4f peak in the survey scan confirms the attachment of Pb species onto the surface of the PANI-NSA@Ni^0 CNs. High resolution spectrum of Pb 4f orbital as displayed in Fig. 9b is comprised of two peaks related to the Pb $4f_{7/2}$ and Pb $4f_{5/2}$ orbitals, respectively. The measured Pb $4f_{7/2}$ peak centred at 138.2 eV binding energy is slightly lesser than the peak at 138.7 eV reported for Pb(II) remediation using resin-supported nano zero valent iron (nZVI) [20]. Conversely, the peak at 143.1 eV is in proximity with the reported binding energy of 143.5 eV for Pb $4f_{5/2}$ [49]. These two peaks can be attributed to the +2 oxidation state of Pb

atom. Regardless of the presence of Pb^0 species in the XRD pattern, its absence from the high resolution XPS spectrum of Pb 4f can be explained by the fact that the air oxidation and surface passivation of the formed Pb^0 directed to the attendance of only Pb(II) oxidized products.

The core level XPS spectrum of Ni 2p in the PANI-NSA@Ni^0 CNs after treatment with Pb(II) is demonstrated in Fig. 9c. The deconvoluted peaks specify that the Ni $2p_{3/2}$ peak with binding energy centred at 855.6 eV is slightly shifted towards lower energy value compared to the Ni $2p_{3/2}$ binding energy peak at 855.8 eV prior to reaction with Pb(II). Additionally, occurrence of peaks at 858.1 eV and 875.6 eV corresponding to the + 3 oxidation state of Ni (NiOOH) suggests involvement of Ni^{2+} species on reduction process of Pb(II) to Pb^0 [44].

Based on the XRD and XPS analyses results the removal mechanism of Pb(II) by PANI-NSA@Ni^0 CNs can be ascribed to a two-step pathway: firstly, Pb(II) ions from aqueous solution efficiently adsorbed onto the surface sites of the adsorbent as represented by the following expression:

$$Ni^0 + 2H_2O \rightarrow Ni^{2+} + H_2 + 2OH^- \quad (12)$$

$$Ni^0 + 2H_2O + 1/2\ O_2 \rightarrow\ Ni^{2+} +\ 4OH^- \quad (13)$$

$$\text{PANI-NSA@Ni(OH)}_2 + \text{Pb(II)} \rightarrow \text{PANI-NSA@Ni(OH)}_2 - \text{Pb(II) (adsorption)} \quad (14)$$

Secondly, most of the adsorbed Pb(II) was reduced to Pb^0 both by electrochemical reduction as well as by electron rich polymer moieties of PANI-NSA@Ni^0 CNs as expressed below:

$$\text{PANI-NSA@Ni(OH)}_2 - \text{Pb(II)} + 2e^- \rightarrow \text{PANI-NSA@Ni(OH)}_2\text{/NiOOH} - Pb^0 \quad (15)$$

Therefore, the presence of co-existing Pb(II) and Pb^0 species on the surface of the PANI-NSA@Ni^0 CNs advocates both adsorption and its subsequent reduction as the major mechanisms associated with Pb(II) removal by the PANI-NSA@Ni^0 CNs as represented graphically in the Scheme 1.

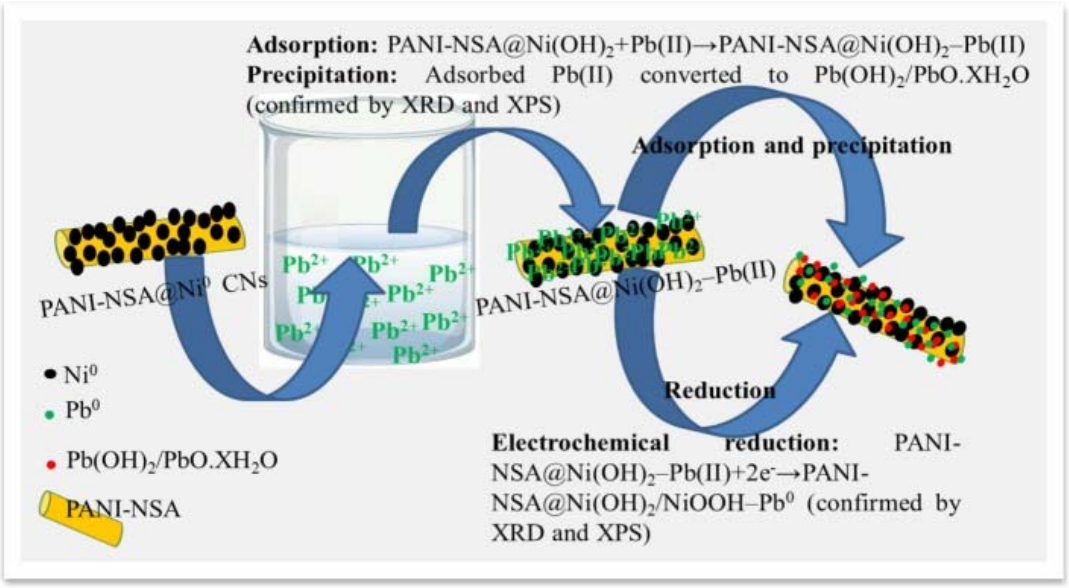

Scheme 1. Plausible mechanism associated with Pb(II) ions removal from aqueous solution.

4. Conclusions

Herein, PANI-NSA@Ni^0 CNs were successfully prepared by reductive immobilization of highly dispersed Ni^0 NPs onto the PANI-NSA nanotubes surface and effectively applied for the efficient removal of Pb(II) ions from aqueous solution. Enhanced Pb(II) removal efficiency (90.9%) was achieved by PANI-NSA@Ni^0 CNs when compared with bare Ni^0 NPs (27.9%) and PANI-NSA nanotubes (13.5%) counterparts. Optimum Pb(II) removal performance was observed at a pH of 5.0 from a 100 mg/L solution using 0.5 g/L dose of PANI-NSA@Ni^0 CNs. Exothermic nature of adsorption was observed with a maximum adsorption capacity of 414.67 mg/g for Pb(II) at 25 °C as obtained from non-linear with Langmuir model fitting of experimental isotherm data. Kinetic investigation revealed that a pseudo-second-order kinetic model was suitable to explain the kinetic mechanism of Pb(II) adsorption onto PANI-NSA@Ni^0 CNs. Co-contaminating metal ions slightly affected the Pb(II) removal performance of PANI-NSA@Ni^0 CNs which recommends its potential application in treating industrial wastewater ladened with other heavy metal pollutants. A mechanistic investigation by XRD and XPS techniques demonstrated adsorption of Pb(II) by deprotonated surface sites of PANI-NSA@Ni^0 CNs and its subsequent reduction to Pb^0 are the prime mechanisms implicated in the present removal process.

Declaration of Competing Interest

The authors declare that they have no known competing financial interests or personal relationships that could have appeared to influence the work reported in this paper.

Acknowledgements

MB is grateful to the University of Pretoria, South Africa, for providing a post-doctoral fellowship. The authors like to acknowledge the chemical engineering department, University of Pretoria, South Africa, for providing infrastructure for the research activity. The authors would also like to thank Prof. VV Srinivasu, University of South Africa, South Africa, for helping to characterize the magnetic property of the adsorbent using PPMS.

References

[1] F. Zan, S. Huo, B. Xi, J. Su, X. Li, J. Zhang, K.M. Yeager. A 100 year sedimentary record of heavy metal pollution in a shallow eutrophic lake, Lake Chaohu, China. J. Environ. Monit., 13 (2011), pp. 2788-2797

[2] S.L. Wang, X.R. Xu, Y.X. Sun, J.L. Liu, H.B. Li. Heavy metal pollution in coastal of South China: a review. Mar. Pollut. Bull., 76 (2013), pp. 7-15

[3] G. Akinci, D.E. Guven, S.K. Ugurlu. Assessing pollution in Izmir Bay from rivers in western Turkey: heavy metals. Environ. Sci., 15 (2013), pp. 2252-2262

[4] M. Fujita, Y. lde, D. Satoetal. Heavy metal contamination of coastal lagoon sediments: fongafale islet, Funafutiatoll, Tuvalu. Chemosphere, 95 (2014), pp. 628-634

[5] Lead poisoning and health, WHO report, 23 August, 2019.

[6] M.T. Alvarez, C. Crespo, B. Mattiasson. Precipitation of Zn(II), Cu(II) and Pb(II) at bench-scale using biogenic hydrogen sulfide from the utilization of volatile fatty acids. Chemosphere, 66 (2007), pp. 1677-1683

[7] F. Fu, Q. Wang. Removal of heavy metals from waste waters: a review. J. Environ. Manage., 92 (2011), pp. 407-418

[8] M. Bhaumik, A. Maity, V.V. Srinivasu, M.S. Onyango. Enhanced removal of Cr(VI) from aqueous solution using polypyrrole/Fe_3O_4 magnetic nanocomposite. J. Hazard. Mater., 190 (2011), pp. 381-390

[9] A.M. Renu, K. Singh. Heavy metal removal from wastewater using various adsorbents: a review. J. Water Reuse Desalination, 7 (2017), pp. 387-419

[10] P. Xu, G.M. Zeng, D.L. Huang, C.L. Feng, S. Hu, M.H. Zhao, C. Lai, Z. Wei, C. Huang, G.X. Xie, Z.F. Liu. Use of iron oxide nanomaterials in wastewater treatment: a review. Sci. Total Environ., 424 (2012), pp. 1-10

[11] Y. Zhang, B. Wu, H. Xu, H. Liu, M. Wang, Y. He, B. Pan. Nanomaterials-enabled water and wastewater treatment. NanoImpact, 3–4 (2016), pp. 22-39

[12] N. Savage, M.S. Diallo. Nanomaterials and water purification: opportunities and challenges. J. Nanopart. Res., 7 (2005), pp. 331-342

[13] H. Ming, S. Zhang, B. Pan, W. Zhang, L. Lu, Q. Zhang. Heavy metal removal from water/wastewater by nanosized metal oxides: a review. J. Hazard. Mater., 211–212 (2012), pp. 317-331

[14] E.M. Hotze, T. Phenrat, G.V. Lowry. Nanoparticle aggregation: challenges to understanding transport and reactivity in the environment. J. Environ. Qual., 39 (2010), pp. 1909-1924

[15] M. Bhaumik, H.J. Choi, R.I. McCrindle, A. Maity. Composite nanofibers prepared from metallic iron nanoparticles and polyaniline: high performance for water treatment applications. J. Colloid Interf. Sci., 425 (2014), pp. 75-82

[16] J. Yang, H. Zhang, M. Yu, I. Emmanuelawati, J. Zou, Z. Yuan, C. Yu. High-content, well-dispersed γ -Fe_2O_3 nanoparticles encapsulated in macroporous silica with superior arsenic removal performance. Adv. Funct. Mater., 24 (2014), pp. 1354-1363

[17] A. Afshar, S.A.S. Sadjadi, A. Mollahossaeini, M.R. Eskandarian. Polypyrrole-polyaniline/ Fe_3O_4 magnetic nanocomposite for removal of Pb(II) from aqueous solution Korean J. Chem. Eng., 33 (2016), pp. 1-9.

[18] F. Elmi, T. Hosseini, M.S. Taleshi, F. Taleshi. Kinetic and thermodynamic investigation into lead adsorption process from wastewater through magnetic nanocomposite Fe_3O_4/CNT. Nanotechnol. Environ. Eng., 2 (2017), pp. 2-13

[19] L. Kuang, M. He, B. Chen, B. Hu. Magnetic Zr-MOFs nanocomposites for rapid removal of heavy metal ions and dyes from water. Chemosphere, 199 (2018), pp. 435-444

[20] S.M. Ponder, J.G. Darab, T.E. Mallouk. Remediation of Cr(VI) and Pb(II) aqueous solutions using supported, nanoscale zerovalent iron. Environ. Sci. Technol., 34 (2000), pp. 2564-2569
[21] X. Zhang, S. Lin, Z. Chen, M. Megharaj, R. Naidu. Kaolinite supported nanoscale zero-valent iron for removal of Pb^{2+} from aqueous solution: reactivity, characterization and mechanism. Water Res., 45 (2011), pp. 3481-3488
[22] S.A. Kim, S. Kamala-Kannan, K.J. Lee, Y.J. Park, P.J. Shea, W.H. Lee, H.M. Kim, B.T. Oh. Removal of Pb(II) from aqueous solution by a zeolite–nanoscale zero-valent iron composite. Chem. Eng. J., 217 (2013), pp. 54-60
[23] W. Zhang, X. Shi, Y. Zhang, W. Gu, B. Li, Y. Xian. Synthesis of water-soluble magnetic graphene nanocomposite for recyclable removal of heavy metal ions. J. Mater. Chem. A, 1 (2013), pp. 1745-1754
[24] L. Ge, W. Wang, Z. Peng, F. Tan, X. Wang, J. Chen, X. Qiao. Facile fabrication of Fe@ MgO magnetic nanocomposites for efficient removal of heavy metal ion and dye from water. Powder Technol., 326 (2018), pp. 393-401
[25] J. Han, L. Wang, R. Guo. Reactive polyaniline-supported sub10-nm noble metal nanoparticles protected by a mesoporous silica shell: controllable synthesis and application as efficient recyclable catalysts. J. Mater. Chem., 22 (2012), pp. 5932-5935
[26] J. Han, J. Dai, L. Li, P. Fang, R. Guo. Highly uniform self-assembled conducting polymer/gold fibrous nanocomposites: additive-free controllable synthesis and application as efficient recyclable catalysts. Langmuir, 27 (2011), pp. 2181-2221
[27] Y.Z. Long, M.M. Li, C. Gu, M. Wan, J.L. Duvail, Z. Liu, Z. Fan. Recent advances in synthesis, physical properties and applications of conducting polymer nanotubes and nanofibers. Prog. Poly. Sci., 36 (2011), pp. 1415-1442
[28] P. Singh, S.K. Shukla. Advances in polyaniline-based nanocomposites. J. Mater. Sci., 55 (2020), pp. 1331-1365
[29] N.R. Tanguy, M. Thompson, N. Yan. A review on advances in application of polyaniline for ammonia detection. Sens. Actuators B, 257 (2018), pp. 1044-1064
[30] J. Banerjee, K. Dutta, M.A. Kader, S.K. Nayak. An overview on the recent developments in polyaniline-based supercapacitors. Polym. Adv. Technol., 30 (2019), pp. 1902-1921
[31] X. Guo, G.T. Fei, H. Su, L.D. Zhang.High-performance and reproducible polyaniline nanowire/tubes for removal of Cr(VI) in aqueous solution. J. Phys. Chem. C, 115 (2011), pp. 1608-1613
[32] J. Han, P. Fang, J. Dai, R. Guo. One-pot surfactantless route to polyaniline hollow nanospheres with in continuous multicavities and application for the removal of lead ions from water. Langmuir, 28 (2012), pp. 6468-6475
[33] M. Bhaumik, C. Noubactep, V.K. Gupta, R.I. McCrindle, A. Maity. Polyaniline/Fe^0 composite nanofibers: an excellent adsorbent for the removal of arsenic from aqueous solutions. Chem. Eng. J., 271 (2015), pp. 135-146
[34] D. Shao, C. Chen, X. Wang. Application of polyaniline and multiwalled carbon nanotube magnetic composites for removal of Pb(II). Chem. Eng. J., 185–186 (2012), pp. 144-150
[35] R. Karthik, S. Meenakshi. Removal of Pb(II) and Cd(II) ions from aqueous solution using polyaniline grafted chitosan. Chem. Eng. J., 263 (2015), pp. 168-177
[36] R. Karthik, S. Meenaksh. Biosorption of Pb(II) and Cd(II) ions from aqueous solution using polyaniline/chitin composite. Sep. Sci. Technol., 51 (2016), pp. 733-742
[37] S. Piri, Z.A. Zanjani, F. Piri, A. Zamani, M. Yaftian, M. Dava. Potential of polyaniline modified clay nanocomposite as a selective decontamination adsorbent for Pb(II) ions from

contaminated waters; kinetics and thermodynamic study. J. Environ. Health Sci. Eng., 14 (20) (2016), pp. 1-10
[38] N.K. Madi, J.B. Wadra, N.J. Al-Thani, A. Alashraf, D. Abdulmalik, I. Al-Qaradawi. Adsorption study of Pb(II) in aqueous medium using polyaniline nanocomposites. J. Vinyl Addit. Technol., 23 (2017), pp. E99-E106
[39] N. Moazezi, M. Baghdadi, M.A. Hickner, M.A. Moosavian. Modelling and experimental evaluation of Ni(II) and Pb(II) sorption from aqueous solutions using a polyaniline/$CoFeC_6N_6$ nanocomposite. J. Chem. Eng. Data, 63 (2018), pp. 741-750
[40] J. Chen, N. Wang, Y. Liu, J. Zhu, J. Feng, W. Yan. Synergetic effect in a self-doping polyaniline/TiO_2 composite for selective adsorption of heavy metal ions. Synth. Met., 245 (2018), pp. 32-41
[41] T. Mahmood, M.T. Saddique, A. Naeem, P. Westerhoff, S. Mustafa, A. Alum. Comparison of different methods for the point of zero charge determination of NiO. Ind. Eng. Chem. Res., 50 (2011), pp. 10017-10023
[42] Z. Zhang, Z. Wei, L. Zhang, M. Wan. Polyaniline nanotubes and their dendrites doped with different naphthalene sulfonic acids. Acta Mater., 53 (2005), pp. 1373-1379
[43] J. Huang, M. Wan. In situ doping polymerization of polyaniline microtubules in the presence of β-naphthalene sulfonic acid. J. Polym. Sci. A: Polym. Chem., 37 (1999), pp. 151-157
[44] M. Bhaumik, V.K. Gupta, A. Maity. Synergetic enhancement of Cr(VI) removal from aqueous solutions using polyaniline@$Ni(OH)_2$ nanocomposites adsorbent. J. Environ. Chem. Eng., 6 (2018), pp. 2514-2527
[45] X.L. Wei, M. Fahlman, A.J. Epstein. XPS study of highly sulfonated polyaniline Macromolecules, 32 (1999), pp. 3114-3117
[46] J. Wang, Q. Zhao, H. Hou, Y. Wu, W. Yu, X. Ji, L. Shao. Nickel nanoparticles supported on nitrogen-doped honeycomb-like carbon frameworks for effective methanol oxidation. RSC Adv., 7 (2017), pp. 14152-14158
[47] R.M. Bozorth. Ferromagnetism. D. Van Nostrand Company Inc, New York (1951)
[48] B.P. Payne, M.C. Biesinger, N.S. McIntyre. The study of polycrystalline nickel metal oxidation by water vapour. J. Electron. Spectros. Relat. Phenomena, 175 (2009), pp. 55-65
[49] T.W. Ng, C.Y. Chan, M.F. Lo, Z.Q. Guana, C.S. Lee. Formation chemistry of perovskites with mixed iodide/chloride content and the implications on charge transport properties. J. Mater. Chem. A, 3 (2015), pp. 9081-9085